RSC Sustainability

ROYAL SOCIETY OF CHEMISTRY

PAPER

View Article Online
View Journal | View Issue

Cite this: *RSC Sustainability*, 2023, **1**, 1833

Towards furfural and biomass char production from *Camellia oleifera* husks using dilute hydrochloric acid pretreatment: a comprehensive investigation on adsorption performance†

Mingyang Hu, Yanyan Yu, Xiaoyan Li, Xinyu Wang and Yun Liu*

This study aimed to revolutionize the conventional lignocellulose refinery approach by capitalizing on the unique composition of *Camellia oleifera* husks, renowned for a high hemicellulose content compared to cellulose and lignin. The complete removal of hemicellulose was successfully achieved using dilute hydrochloric acid (HA) under optimized conditions (130 °C, 500 rpm, 40% solids, and 1 h). The resulting xylose solution, derived from the hemicellulose, served as a valuable resource for furfural production. Remarkably, S-8 macroporous resin exhibited exceptional adsorption properties for furfural, with an impressive maximum adsorption capacity of 335.68 mg g^{-1}, adhering to the Langmuir model; furthermore, the residual husk material was converted into biomass char (BC), which underwent characterization using FTIR, SEM, and BET techniques. The BC displayed remarkable adsorption capabilities for methylene blue dye, with a maximum theoretical adsorption capacity of 250.63 mg g^{-1}. Notably, the dilute HA solution and S-8 macroporous resin could be successfully recycled up to five cycles, as the furfural yields consistently exceeded 70%, and the S-8 resin fully regained its initial adsorption capacity after the regeneration process. Mass balance analysis showed that 100 g of *C. oleifera* husks had the potential to yield 11.3 g of furfural and 35.7 g of BC. These findings unlock promising avenues for sustainable biomass valorization, representing a significant step forward in utilizing *C. oleifera* husks efficiently.

Received 8th June 2023
Accepted 21st August 2023

DOI: 10.1039/d3su00181d

rsc.li/rscsus

Sustainability spotlight

Camellia oleifera husks are a by-product of the oil tea processing process. The resourceful use of oil tea shells can not only improve its own added value but also solve the problem of environmental pollution brought about by it, in line with the development trend of sustainability. Due to the unique composition of oil tea shells. We used dilute hydrochloric acid to hydrolyze hemicellulose for the preparation of FF and adsorbed it through S-8 macroporous resin, using organic solvents to resolve and obtain a highly concentrated FF solution. The remaining solid residue was used to prepare biomass-activated carbon for the adsorption of MB dyes in printing and dyeing wastewater. The dilute hydrochloric acid solution, S-8 macroporous resin, and organic solvents can be recycled throughout the process. In addition, this research is in line with the UN sustainable development goals for clean water and sanitation (SDG 6), and affordable clean energy (SDG 7).

1. Introduction

Lignocellulosic biomass, a pivotal renewable resource, offers immense potential as a future alternative to fossil fuels.[1] The three primary components of lignocellulose are cellulose (38–50%), hemicellulose (23–32%), and lignin (12–25%).[2] Nevertheless, the proportions of these components can vary depending on the source or nature of the material. For instance, wheat straw comprises 40.4% cellulose, 28.2% hemicellulose, and 17.6% lignin,[3] whereas dewaxed poplar consists of 48.7% cellulose, 25.0% hemicellulose, and 24.9% lignin,[4] and eucalyptus contains 43.5% cellulose, 17.1% hemicellulose, and 26.3% lignin.[5] Consequently, tailoring the utilization of biomass based on its specific compositions becomes crucial for biomass refinery.

Current biomass pretreatment technologies fall into three main groups, physical, chemical, and biological treatments. Each category exhibits varying specificity for carbohydrates and lignin, making them more or less effective for different types of biomass.[6] However, it is essential to recognize that enzymatic saccharification of cellulose followed by fermentation for

Beijing Key Laboratory of Bioprocess, College of Life Science and Technology, Beijing University of Chemical Technology, Beijing, 100029, China. E-mail: liuyun@mail.buct.edu.cn; liuyunprivate@sina.com; Fax: +86-010-64421335; Tel: +86-010-64416428

† Electronic supplementary information (ESI) available. See DOI: https://doi.org/10.1039/d3su00181d

bioethanol production, while common for feedstock with a high cellulose content, often overlooks the potential value of hemicellulose and lignin.[7] The enzymatic fermentation of cellulose faces challenges such as by-product inhibitors during pretreatment, loss of sugar breakdown, and the requirement of high enzyme loads for hydrolysis. For example, Yu *et al.* discovered that cellulose treated with formic acid was unsuitable for enzymatic fermentation.[8] As an alternative, they developed a cellulose-based PdAg bimetallic catalyst for hydrogen production, showing promising results. Similarly, Mashhadimoslem *et al.* developed an oxidized porous carbon adsorbent using walnut shells, demonstrating excellent adsorption capacity for oxygen and nitrogen.[9] To full exploit the value of lignocellulose, it is crucial to tailor its utilization based on its unique characteristics. This calls for the development of flexible and integrated biorefinery technologies, which can efficiently produce biochemicals and biomaterials from renewable biomass resources. Such advancements are key to achieving a transition from a petroleum economy to a biomass economy.[10]

Furfural (FF) stands as a crucial biomass platform compound, holding the potential for catalytic conversion into fuels and high-value-added chemicals.[11] When biomass hemicellulose undergoes hydrolysis at specific temperatures and under acidic conditions, it produces pentose, which subsequently dehydrates to form FF.[1] This versatile compound finds application in preparing essential solvents like furfuryl alcohol, furfuric acid, tetrahydrofuran, γ-pentyl lactone, pyrrole, and tetrahydropyrrole, as well as being widely utilized in pharmaceuticals, pesticides, and bio-based plastics.[12] Despite its many uses, several existing FF production processes face limitations. Firstly, these processes yield only about 50% of the theoretical value and require long reaction times.[13] Secondly, challenges arise in wastewater management during the production process, leading to equipment corrosion and difficulties in FF separation.[14] Thirdly, substantial energy consumption is observed due to the use of steam as both the heat source and extractant. Steam consumption in FF production can be 30–50 times higher than the FF output, making it the most significant cost factor. Additionally, the low purity of crude FF increases the cost of subsequent refinement and purification steps.[15] A key step in the FF production process is the fast and efficient separation of FF from aqueous solution. Some research efforts have focused on this aspect. Li *et al.* successfully adsorbed FF using metal–organic framework materials (MOFs) with a maximum adsorption amount of 60.79 mg g^{-1}, while another study showed that COF-300 is an efficient FF adsorbent, reaching adsorption equilibrium within 10 seconds and with a maximum adsorption capacity of 567.8 mg g^{-1}.[16] Additionally, Xiang *et al.* synthesized magnetic nanoparticles as adsorbents for FF using oxidized alkaline lignin, which reached adsorption equilibrium at 60 min, with a FF removal rate of 53.12% and a maximum adsorption capacity of 20.48 mg g^{-1}.[17] Hence, exploring the development of new FF adsorbent materials to enhance the efficiency and purity of the FF production process appears as a promising direction.

Activated carbon is an amorphous carbon-based material known for its high specific surface area, porosity, and abundance of functional groups. It finds extensive utilization in wastewater treatment for adsorbing heavy metals, dyes, and other toxic substances.[18] However, the high cost of commercially available activated carbon, primarily derived from non-renewable coal, hinders its widespread application.[19] Consequently, research has shifted towards biomass char (BC) prepared from renewable biomass resources, which is expected to replace commercial activated carbon and reduce dependence on coal-derived fossil energy.

Methylene blue (MB) is a widely used water-soluble azo dye, existing as a cationic quaternary amine salt in water. It possesses high chromaticity and is resistant to biodegradation. When MB dye-containing wastewater enters the aquatic environment, it disrupts the ecological balance by affecting the photosynthesis of aquatic plants and causes severe pollution.[20] Adsorption is a well-developed method for dye removal from wastewater, due to the process simplicity and lower cost involved compared to other processes.[21–23] For instance, Jawad *et al.* successfully prepared activated carbon from mangosteen peels using microwave-assisted phosphoric acid activation.[24] This activated carbon showed an impressive adsorption capacity of 163.6 mg g^{-1} for MB dye in textile wastewater. Similarly, Baytar *et al.* utilized microwave and $ZnCl_2$ activation to prepare activated carbon from sunflower seed shells, demonstrating a high adsorption capacity of 240 mg g^{-1} for MB dye.[25] These examples highlight the remarkable adsorption potential of lignocellulosic biomass through simple carbonization and chemical activation processes.

Camellia oleifera husks, a byproduct of edible tea oil production, contain a significant amount of cellulose, hemicellulose and lignin, endowing them with promising potential applications, such as furfural (FF) and activated carbon production. Comparison to other lignocellulose biomass, *C. oleifera* husks exhibit higher levels of hemicellulose and lower levels of cellulose. The comprehensive utilization of hemicellulose in *C. oleifera* husks can substantially increase their value. Therefore, this study aimed to extract and purify FF derived from *C. oleifera* husks, building upon the previous research conducted by Liu *et al.*[26] Initially, we employed S-8 macroporous resin to adsorb FF, and the adsorption mechanism and performance were thoroughly examined using adsorption isotherms, kinetics, and thermodynamics. Subsequently, we desorbed the adsorbed S-8 macroporous resin using 2-methyl tetrahydrofuran (2-Me-THF), and FF was obtained from the resulting mixture by vacuum distillation. Additionally, the recovery and recycling of the diluted HA solution and S-8 macroporous resin were also evaluated.

To enhance the value of *C. oleifera* husks, we prepared biomass char from the solid residue left after FF production, utilizing $ZnCl_2$ activation. This resulting biomass char was tested for its efficiency in adsorbing MB dye. The study extensively examined the adsorption performance and mechanism of the biomass char, employing various adsorption models. The exceptional adsorption capacity of MB by the biomass char can be attributed to its unique structure, which was confirmed

through Fourier Transform Infrared (FTIR), scanning electron microscopy (SEM), and Brunauer–Emmett–Teller (BET) analyses. As a result, this study uncovers exciting prospects for the tailored application and utilization of *C. oleifera* husks, particularly in China.

2. Materials and methods

2.1. Materials

The *C. oleifera* husks utilized in this study were generously provided by Guizhou Buyi Liji oil tea industry Co., Ltd, China. To prepare them for analysis, the husks were crushed to a size of 40 mesh and subsequently dried at 80 °C. The cellulose, hemicellulose, and lignin contents of *C. oleifera* husks were determined to be 22.6 ± 0.52%, 36.4 ± 0.84%, and 38.9 ± 0.83%, respectively, following the methods provided by the National Renewable Energy Laboratory (NREL).[27] For the study, all reagents used, including sulphuric acid (SA) and hydrochloric acid (HA), were purchased from Beijing Tongguang Fine Chemical Company, China. Chromatographic-grade glucose, xylose, and FF were obtained from J & K Science Ltd, Pforzheim, Germany, while 2-methyltetrahydrofuran (2-Me-THF), magnesium chloride ($MgCl_2$), and zinc chloride ($ZnCl_2$) were acquired in analytical purity from J & K Beijing Science Ltd, China. The S-8 macroporous resin used in the study was purchased from the Beijing Market, China. It is essential to note that all chemical reagents mentioned in this work are of analytically pure quality.

2.2. Production of FF from *C. oleifera* husks through dilute HA pretreatment

The production of FF was slightly modified based on previous research work.[26] To initiate the reaction, 2.5 g of powered *C. oleifera* husks were mixed with a 10% dilute HA solution in a 100 mL glass pressure-resistant flask, using a solid-to-liquid ratio of 1 : 20 (mass/volume). The mixture was then heated to a temperature of 130 °C and agitated at 500 rpm for 1 h. After the reaction completion, the filtrate residue was separated from the mixture through filtration. The filtrate was then combined with a $MgCl_2$ catalyst at a concentration of 15.0 g L^{-1}, and the resulting solution was introduced into a stainless steel reactor, where it was subjected to a temperature of 180 °C for 1.5 h to produce FF. Once the reaction was complete, the filtrate containing FF was filtered again to remove any impurities and stored in a 50 mL conical flask, protected from light. The residue obtained from filtration was dried at 80 °C and used for the preparation of biomass char in the subsequent experiment.

2.3. FF adsorption experiments and kinetics using S-8 macroporous resin

In a typical adsorption experiment, 7.5 g of wet weight S-8 macroporous adsorbent resin was added to the FF solution, which had a volume of 100 mL obtained from the previous step. The adsorption process was conducted at a temperature of 30 °C and a stirring speed of 220 rpm until equilibrium was reached. At this point, a sample was taken and filtered, and the concentration of FF in the solution was determined using a UV-Vis spectrophotometer (Shimadzu) at its maximum absorbance wavelength of 276 nm. The amount of FF adsorbed at equilibrium (Q_e, mg g^{-1}) was calculated using the following eqn (1):

$$Q_e\ (\%) = \left(\frac{C_0 - C_e}{M}\right) \times V \quad (1)$$

where Q_e is the amount of FF adsorbed at equilibrium (mg g^{-1}); C_0 is the initial concentration of FF in the solution (mg L^{-1}); C_e is the concentration of FF in the filtrate at equilibrium (mg L^{-1}); M is the adsorbent resin mass (g); V is the volume of the solution (L).

A series of experiments were conducted to investigate the adsorption kinetics, isotherms, and thermodynamics of FF on the S-8 macroporous adsorbent resin. The adsorption kinetics experiments involved preparing FF specimens with a concentration of 5 g L^{-1} and conducting adsorption at 30 °C using 7.5 g of the adsorbent for 30 min. Samples were collected at intervals of 5, 10, 15, 20, and 30 min for the subsequent analysis.

In the adsorption isotherm experiments, FF solutions with concentrations ranging from 1 to 5 g L^{-1} were prepared and subjected to adsorption for 30 min at a temperature of 30 °C.

To examine the adsorption thermodynamics, experiments were performed at various temperatures (20, 30, 40, 50, and 60 °C) using a fixed FF concentration of 5 g L^{-1} and an adsorption time of 30 min.

Furthermore, adsorbent addition experiments were conducted by introducing different amounts of S-8 macroporous resin (3.5 g, 4.5 g, 5.5 g, 6.5 g, and 7.5 g) at a concentration of 5 g L^{-1} and a temperature of 30 °C for 30 min. These experiments aimed to characterize and predict the adsorption behavior and rates of FF on the S-8 macroporous adsorbent resin.

2.4. FF desorption and extraction

In this study, the adsorbed S-8 macroporous resin was subjected to desorption using various solvents, including ethanol, methanol, dichloromethane, ether, and 2-Me-THF. The desorption process was carried out as follows: the adsorbed S-8 macroporous resin was placed in a 250 mL conical flask and mixed with 50 mL of the chosen solvent. The mixture was then maintained at 30 °C for 1 h to facilitate dissolution. Subsequently, the S-8 macroporous resin was filtered out and returned to the conical flask for a secondary extraction. The resulting solutions from both extractions were combined, and the concentration of FF in the combined solution was determined. The resolution rate was calculated based on the mass ratio. Finally, the obtained filtrate was subjected to a rotary evaporator at 60 °C until no solvent remained.

2.5. Dilute HA solution recycling

The dilute HA solution utilized during the pretreatment process was recycled by subjecting the FF solution to filtration after adsorption with S-8 macroporous resin, enabling its re-utilization. The experimental procedure remained unchanged from the description in Section 2.2, except for the substitution of the 10% dilute HA solution with the retrieved diluted HA solution.

2.6. S-8 macroporous resin regeneration and recycling

When the S-8 macroporous resin became saturation with adsorbed FF, its adsorption capacity diminished, necessitating a regeneration process to restore its effectiveness. The regeneration process involved immersing the adsorbed S-8 macroporous resin in a 100 mL solution of 5% HA for 3 h. Subsequently, the resin was thoroughly washed with deionized water for 3 h until it reached a neutral pH. Following this, an additional washing step with 100 mL of 5% NaOH was performed for 3 h. Finally, the resin underwent another rinse with deionized water until it reached a neutral state.

2.7. Preparation of biomass char (BC) from the solid residue

BC was prepared following the methodology of Xue *et al.* with additional improvements.[18] The process involved the dilute hydrolysis of HA, resulting in a solid residue, which was then dried at 105 °C in an oven. Next, 5 g of the dried residue was mixed thoroughly with a 4 mol L^{-1} $ZnCl_2$ solution under stirring. The resulting mixture was subsequently dried at 80 °C and transferred to a porcelain boat within a high-temperature tube furnace. The temperature was gradually raised to 500 °C at a rate of 10 °C min^{-1}, and the material was calcined for 3 h to obtain BC. The obtained BC underwent a series of washing steps using a 2 mol L^{-1} HA solution and distilled water until the filtrate reached a neutral pH. Afterwards, it was dried at 105 °C. Finally, the dried BC was finely ground and crushed before being stored and preserved. The yield of BC was determined using eqn (2):

$$\text{Biomass char yield } (\%) = \frac{\text{mass of residue fter calcination (g)}}{\text{mass of residue before calcination (g)}} \times 100 \quad (2)$$

2.8. Adsorption experiments of methylene blue (MB) dye on BC

The experimental procedure related to MB adsorption on BC involved several steps. Firstly, different concentrations of MB dye solutions (15, 25, 35, 45, and 55 mg L^{-1}) were prepared. Subsequently, 30 mg of BC was introduced into a conical flask containing 100 mL of MB dye solution. The BC adsorption experiments were conducted at 30 °C and 220 rpm. At regular intervals, samples were collected and suitably diluted to determine the concentration of the unabsorbed dye. The concentration of MB was measured by assessing the absorbance at 665 nm using a UV-Vis spectrophotometer. Once adsorption equilibrium was achieved, the adsorption capacity of BC was calculated using the aforementioned eqn (1).

Furthermore, to examine the effect of the pH of the MB dye solution on BC adsorption, solutions of 1 mol per L NaOH and HCl were utilized to adjust the pH of the MB solution to values ranging from 2 to 12. The adsorption process for this set of experiments was identical to the one described above.

This comprehensive approach allowed for a systematic investigation of the BC adsorption performance under different MB dye concentrations and varying pH conditions.

2.9. Structural characterization of biomass char

SEM photographs of BC were taken using a scanning electron microscope-cold field (S-4700, Hitachi). N_2 adsorption–desorption measurements were conducted using a multi-station specific surface area and pore size analyzer (BET-ASAP2460, USA) to determine the specific surface area, pore size, and pore volume of BC. The pore size was calculated employing the BJH method. Additionally, the FTIR spectra of BC were acquired using a Cary 600 series FTIR spectrometer (IRAffinity-1S, Shimadzu, Japan) with the KBr press method, both before and after the adsorption of MB dye.

The point zero charge (pH_{pzc}) of BC was determined using the pH drift method.[22] Typically, in a conical flask, 50 mL of NaCl (0.01 M) solution was added, and the pH was adjusted to 3, 4, 5, 6, 7, 8, and 9 using 0.1 mol per L NaOH solution and HCl solution, respectively. Subsequently, 15 mg of BC was added to the flask, and the reaction mixture was shaken for 24 h at 22 °C. At the end of the reaction, the final pH was recorded. The ΔpH represented the difference between the initial pH and final pH, and the intersection of the curve with the *x*-axis provided the pH_{pzc} of BC.

2.10. Data statistics

All experiments were performed in triplicate to ensure reliable results, and the data obtained are presented as mean ± standard deviation (SD) to provide a measure of the data's variability. Graphs and curves illustrating the experimental results were generated using Origin software, version 9.0.0, facilitating clear visualization and analysis of the data.

3. Results and discussion

3.1. Hemicellulose hydrolysate production from *C. oleifera* husks through dilute HA pretreatment

This study aimed to improve the dilute HA treatment of husks based on previous research by Liu *et al.*[26] Typically, a 6% HA solution was used at a high temperature of 170 °C for 1 h to remove hemicellulose from the husks. In contrast, our present study utilized an oil bath and stirring, allowing us to use a lower temperature of 130 °C. This not only reduced the overall process cost but also enhanced the pretreatment efficiency. The effect of reaction temperature on the pretreatment efficiency was investigated, and the results are presented in Fig. 1a. At 130 °C and 500 rpm, the hemicellulose removal rate reached 100%, and the

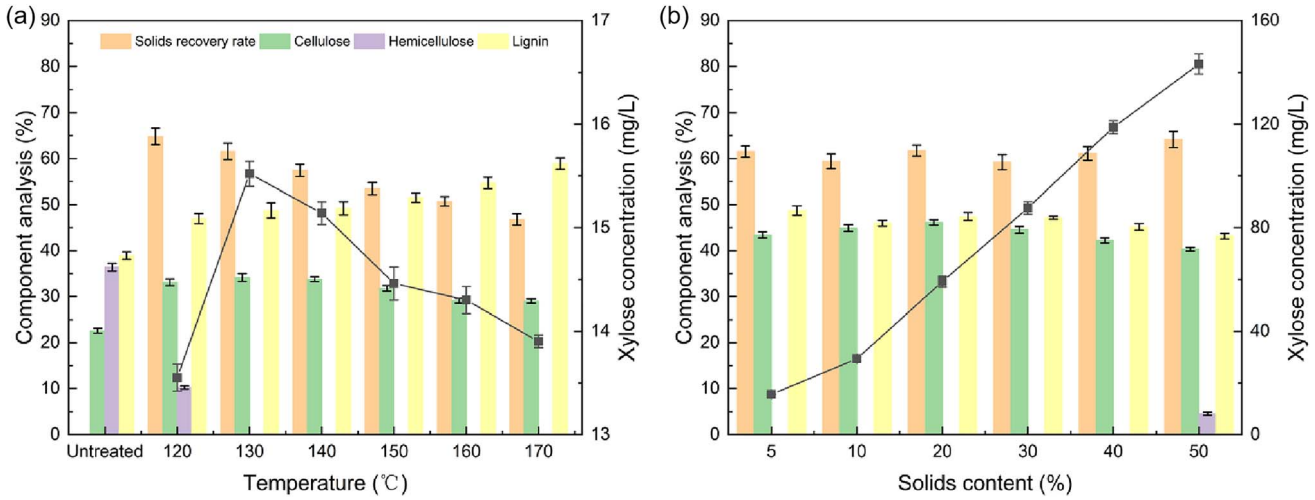

Fig. 1 Dilute HA treatment of husks: (a) composition and filtrate of treated husks at different temperatures and (b) composition and filtrate analysis of husks at different solid loadings.

xylose concentration was 15.52 mg L^{-1}. These positive outcomes were attributed to improved solid/liquid contact and accelerated reaction rates facilitated by stirring, which aligned with the findings from Guo *et al.* research.[28]

Furthermore, the impact of solid loading on the pretreatment efficiency was also investigated, as depicted in Fig. 1b. The study explored solid loads ranging from 5% to 50% and a consistent increase in xylose concentration was observed with higher solid loading. Remarkably, even at a solid loading of 40%, the pretreated husk residue showed no remaining hemicellulose. This highlighted the significance of high solid loading in biomass refineries, as demonstrated by previous research.[29] Moreover, at a solid loading of 50%, only 4.52% hemicellulose was detected, accompanied by a substantial xylose concentration of 143.21 mg L^{-1}. These findings indicated that the system could handle higher solid loading without compromising cost-effectiveness. In summary, the modifications implemented in this study for the dilute HA pretreatment of husks resulted in improved hemicellulose hydrolysis efficiency and reduced process costs.

3.2. Enhancing FF production: adsorption and desorption of hydrolysate using S-8 macroporous resin

This study investigated the production of FF through the reheating and dehydration of hemicellulose hydrolysate, specifically xylose solution. While previous research has already determined the dehydration factors for converting xylose into FF, our main focus is on exploring the adsorption and separation of FF. Experimental findings reveal a promising FF yield of 72.3% using a 10% dilute HA solution at 180 °C for 90 min.

The S-8 macroporous resin adsorbent is a styrene-based polar copolymer with a diethylene benzene backbone structure, and its properties are detailed in the ESI.† The presence of the benzene ring attached to the main chain contributes to a uniform electron distribution, resulting in a robust adsorption capacity for molecules with similar characteristics and cyclic aromatic compounds. This capacity becomes more pronounced as the adsorbed molecule's lipophilicity increases. Operating effectively at temperatures up to 150 °C, the S-8 resin exhibits outstanding selectivity for organic substances and remains unaffected by inorganic salts. Moreover, it can be easily regenerated using solvents such as water, dilute acid, dilute alkali, or low-boiling-point organic solvents like methanol, ethanol, and dichloromethane. Typically, the S-8 resin finds application in the extraction and separation of antibiotics, herbal medicines, and the treatment of organic wastewater. Given its promising properties, in this study, the S-8 macroporous resin was chosen as an ideal adsorbent for FF. The adsorption process and mechanism were thoroughly analyzed by investigating adsorption isotherms, kinetics, and thermodynamics, and the results are presented in Fig. 2.

3.2.1. Adsorption isotherm of FF on S-8 macroporous resin. In this study, the adsorption isotherms of S-8 macroporous resin on FF were investigated at three different temperatures: 20 °C, 30 °C, and 40 °C. The results of these investigations are depicted in Fig. 2a and b. Two primary adsorption isotherm models, namely the Langmuir and Freundlich models, were employed to analyze the data. The Langmuir model assumes a monolayer adsorption process, where the energy at all adsorption sites is identical, and there is no interaction between the adsorbed molecules. On the other hand, the Freundlich model describes an adsorption isotherm with an uneven surface energy, where the adsorption sites are located on heterogeneous surfaces with varying energies. The Freundlich model is commonly applied in environments where concentrations are not high, making it suitable for this study.

By employing these two models, we aimed to gain a comprehensive understanding of the adsorption behavior of FF on the S-8 macroporous resin at different temperatures. The insights from these analyses contribute significantly to our knowledge of the adsorption process and help optimize the efficiency of FF production.

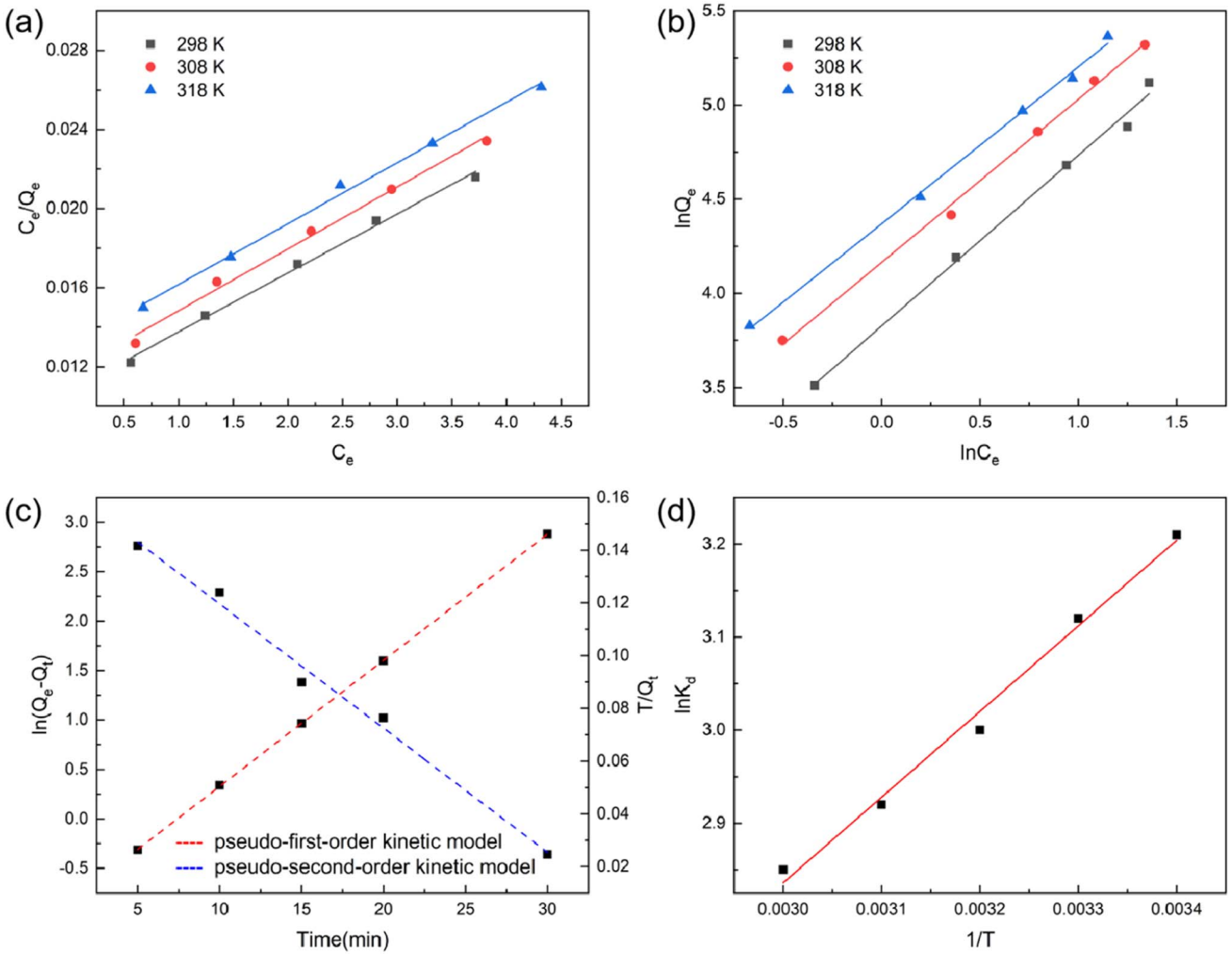

Fig. 2 FF adsorption performance over S-8 macroporous resin. (a) Langmuir adsorption isotherm model at different temperatures, (b) Freundlich adsorption isotherm model at different temperatures, (c) pseudo-first-order and pseudo-second-order adsorption kinetic model curves, and (d) adsorption thermodynamic curve.

Table 1 Adsorption isotherm parameters for FF adsorption on S-8 macroporous resin

Temperature (°C)	Langmuir model			Freundlich model		
	Q_m	K_L	R^2	n	K_F	R^2
20	335.68	0.235	0.996	1.196	78.965	0.992
30	324.49	0.268	0.993	1.153	64.328	0.987
40	319.57	0.276	0.996	1.103	45.879	0.984

Table 1 displays the R^2 values obtained from fitting the Langmuir and Freundlich models at different temperatures. For the Langmuir model, the R^2 values were found to be 0.996, 0.993, and 0.996 at 20 °C, 30 °C, and 40 °C, respectively. On the other hand, the R^2 values for the Freundlich model were 0.984, 0.987, and 0.992 at the same temperatures. The higher R^2 value observed for the Langmuir model indicates a better fit of the adsorption data for FF on S-8 macroporous resin using the Langmuir model. Furthermore, based on the Langmuir model, the maximum adsorption capacity (Q_m) was determined to be 335.68 mg g^{-1} at an adsorption temperature of 40 °C. This finding signifies the highest capacity of the S-8 macroporous resin to adsorb FF at this particular temperature.

3.2.2. Adsorption kinetics of FF on S-8 macroporous resin. The adsorption kinetic data for FF adsorption on S-8 macroporous resin were analyzed using two kinetic models: the pseudo-first-order and pseudo-second-order models. The kinetic eqn (3) and (4) were employed to calculate the kinetic parameters.

$$\ln(Q_e - Q_t) = \ln Q_e - k_1 t \quad (3)$$

$$\frac{T}{Q_t} = \frac{1}{K_2 Q_e^2} + \frac{T}{Q_e} \quad (4)$$

where Q_e and Q_t are the adsorption amounts at equilibrium and at any time t (min), respectively; k_1 is the rate constant for the pseudo-first-order equation (min^{-1}). k_2 is the rate constant for the pseudo-second-order equation (g (mg^{-1} min^{-1})).

By employing the experimental data to fit these kinetic models, it becomes possible to determine the kinetic parameters and conduct a comparative evaluation of the adsorption behavior of FF on S-8 macroporous resin. Fig. 2c depicts the adsorption kinetics of S-8 macroporous resin on FF, which were subsequently analyzed using both the pseudo-first-order and pseudo-second-order kinetic models. The pseudo-first-order model is typically employed to investigate the initial adsorption phase, whereas the pseudo-second-order model is applied to describe the entire adsorption process.

The pseudo-first-order and pseudo-second-order adsorption kinetic constants, along with their corresponding R^2 values, can be found in the ESI.† The calculated Q_1 value using the pseudo-first-order equation was 30.57 mg g^{-1}, whereas the pseudo-second-order equation yielded a calculated Q_2 value of 209.21 mg g^{-1}. It is essential to highlight that the adsorption capacity obtained from the pseudo-first-order equation exhibited a significant deviation from the experimental value. In contrast, the pseudo-second-order equation provided a value that closely matched the experimental adsorption capacity. Based on these results, it is reasonable to conclude that the pseudo-second-order model is more appropriate for analyzing the adsorption behavior of FF on S-8 macroporous resin.

3.2.3. Adsorption thermodynamics of FF on S-8 macroporous resin. Eqn (5)–(7) were utilized to compute the thermodynamic parameters, namely Gibbs free energy (ΔG), enthalpy change (ΔH), and entropy change (ΔS). The specific values of these parameters can be referenced in Table S3.†

$$\Delta G = -RT \ln K_d \quad (5)$$

$$K_d = \frac{Q_e}{C_e} \quad (6)$$

$$\ln K_d = \frac{\Delta S}{R} - \frac{\Delta H}{RT} \quad (7)$$

where K_d denotes the equilibrium constant, T denotes the adsorption temperature (K) and R denotes the universal gas constant (8.314 J ($mole^{-1}$ K^{-1})).

According to the principle of thermodynamics, it is evident that ΔG assumes negative values at different temperatures, indicating that the adsorption of FF by the S-8 macroporous resin is a spontaneous process. Moreover, ΔH is found to be negative, signifying that the adsorption process is exothermic. This observation aligns with the predicted decrease in adsorption capacity as the temperature increases, as illustrated in the adsorption isotherms (Fig. 2a and b). Similar findings were reported by ref. 16. Additionally, the positive value of ΔS suggests that the S-8 macroporous resin exhibits a strong affinity for FF, and the stoichiometry increases during the adsorption process.

3.2.4. FF desorption from S-8 macroporous resin with organic solvents. In this study, the desorption of FF adsorbed on S-8 macroporous resin was conducted using five different solvents: methanol, ethanol, dichloromethane, 2-Me-THF, and acetone. The resolution rates achieved with these solvents can be found in the ESI.† Notably, 2-Me-THF exhibited the highest resolution rate at 76.1%, whereas methanol showed the lowest rate at 35.7%. The observed differences in resolution rates can be attributed to the polarity of the solvents. FF, being a less polar compound, is more easily dissolved by solvents with lower polarity. Moreover, the compatibility of solvent–solute polarity is a crucial factor to consider. Solutes generally dissolve more effectively in solvents with similar polarity due to stronger intermolecular forces. This favorable interaction at the molecular level facilitates better dissolution. In the case of FF, methanol and ethanol, being polar solvents, have lower resolving power for FF and may also contribute to the degradation of FF, as noted in ref. 30.

3.2.5. Recycling and re-utilization. Recovery and recycling play vital roles in the biorefining industry as they contribute to cost reduction, resource conservation, and pollution prevention. In this study, the dilute HA solution, S-8 macroporous resin, and 2-Me-THF were all successfully recovered and recycled, highlighting the industry's commitment to minimizing waste.

The hydrolysis efficiency of hemicellulose in the dilute HA solution remained satisfactory even after undergoing five cycles (see the ESI†). Solid recovery rates ranging from 50.40% to 55.49% were observed, with solid residues containing 41.92% to 45.29% cellulose and 54.15% to 58.15% lignin. Additionally, the production of FF was consistent in the range from 66.92% to 74.77% across multiple cycles. These findings suggested that the dilute HA solution maintained stability and retained its ability for multiple recovery and recycling. The stable recycling effect can be attributed to the unchanged pH of the dilute HA solution after use. It is important to note that hemicellulose typically undergoes rapid hydrolysis under acidic or high-temperature conditions, further highlighting the effectiveness of the recycling process in maintaining the solution's integrity.

Furthermore, the S-8 macroporous resin was successfully recovered for recycling purposes. The adsorption capacity of the regenerated S-8 macroporous resin (193.26 mg g^{-1}) was found to be comparable to that of the fresh S-8 macroporous resin (224.15 mg g^{-1}) (see the ESI†). This significant result indicates that the adsorbent resin can be effectively regenerated through a simple process, making it a practical and cost-effective option for the biorefinery industry. The ability to recycle and reuse the S-8 macroporous resin further enhances the sustainability and efficiency of the biorefining process. By employing such recycling practices, valuable resources are conserved, and waste generation is minimized, reinforcing the environmentally friendly nature of the overall approach.

3.3. Preparation of BC for MB dye adsorption

To optimize the utilization of *C. oleifera* husks, the solid residue obtained after the dilute HA treatment was subjected to carbonization, resulting in the generation of BC. This biomass char was extensively studied to evaluate its adsorption capacity for MB dye, with a specific focus on adsorption kinetics, isotherms, and thermodynamics. The outcomes of these investigations are depicted in Fig. 3. The study's findings underscore the substantial potential of biomass char as a key element in the removal of dyes, thus highlighting its promising role in various dye removal applications.

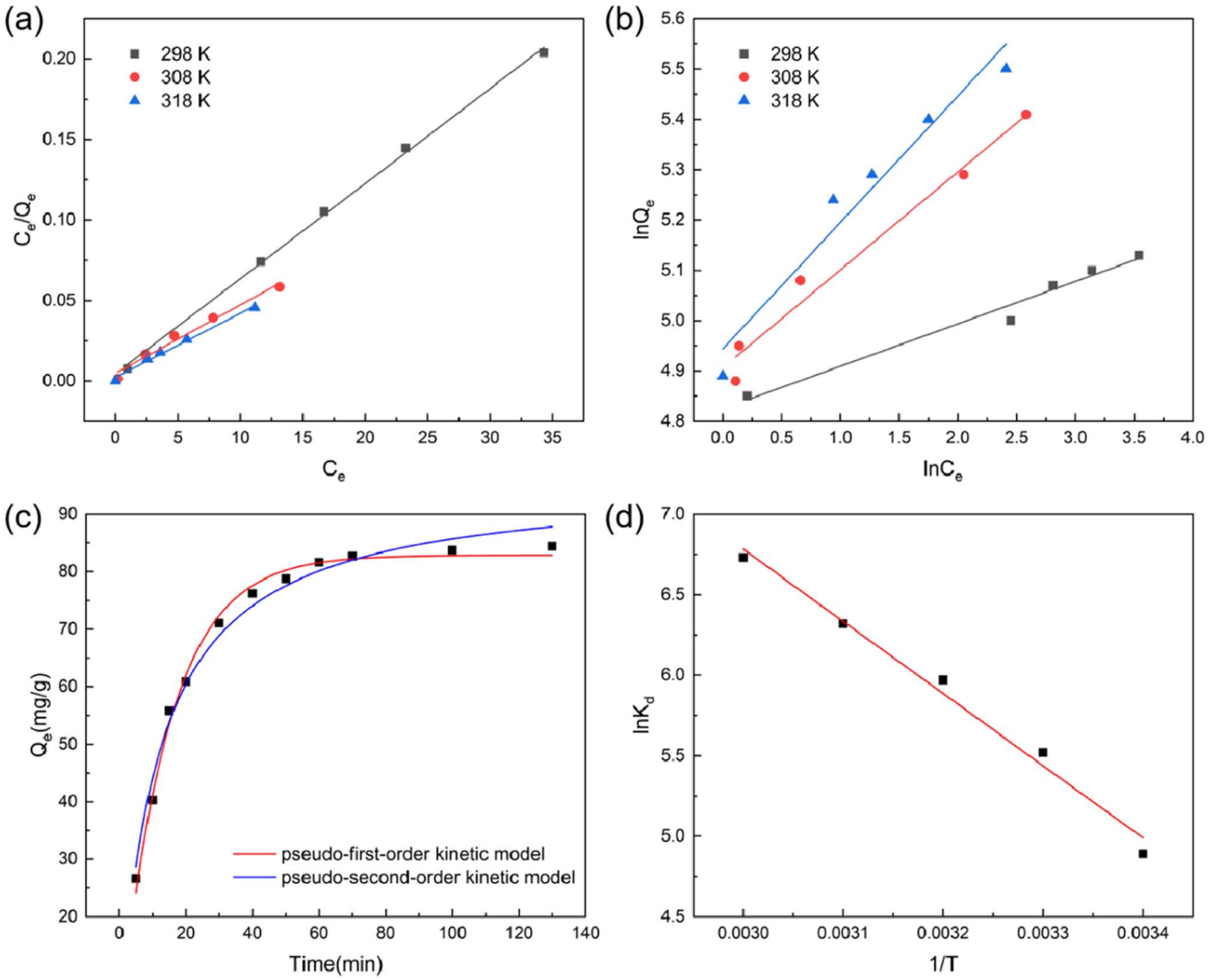

Fig. 3 MB dye adsorption performance on the as-prepared biomass char from *C. oleifera* husks. (a) Langmuir adsorption isotherm model at different temperatures, (b) Freundlich adsorption isotherm model at different temperatures, (c) pseudo-first-order and pseudo-second-order adsorption kinetic model curves, and (d) adsorption thermodynamic curve.

3.3.1. Adsorption isotherm of BC for MB dye. The adsorption behavior and mechanism of BC for MB dye were thoroughly investigated by fitting the adsorption isotherm data using two models: the Langmuir and Freundlich models (Fig. 3a and b). The primary goal of this analysis was to optimize the adsorption efficiency and gain insights into the adsorption behavior of BC concerning MB dye removal. By employing the adsorption isotherm models, the adsorption capacity and efficiency of BC in removing MB dye from solution were evaluated. The experiments were conducted using various initial concentrations of MB dye, ranging from 35 to 75 mg L^{-1}, and at temperatures of 20 °C, 30 °C, and 40 °C. The Langmuir equation (eqn (8)) and Freundlich equation (eqn (9)) were applied to establish linear equations for the purpose of data analyses. These models offer valuable insights into the adsorption process and provide a basis for understanding the interaction between BC and MB dye in the solution.

$$\frac{C_e}{Q_e} = \frac{C_e}{Q_m} + \frac{1}{K_L Q_m} \quad (8)$$

$$\ln Q_m = \ln K_F + \frac{1}{n} \ln C_e \quad (9)$$

where Q_e is the adsorption amount at adsorption equilibrium (mg g^{-1}), Q_m is the maximum adsorption amount of biomass carbon (mg g^{-1}), C_e is the concentration of MB dye at adsorption equilibrium (mg L^{-1}), and K_L is the Langmuir model adsorption constant (L mg^{-1}), K_F is the Freundlich model adsorption sorption constant ((mg g^{-1}) (L mg^{-1})$^{1/n}$), and n is an empirical constant in the Freundlich model.

Table 2 presents the Langmuir and Freundlich isotherm adsorption constants along with their corresponding R^2 values. The data clearly indicate that the Langmuir adsorption model offers a superior fit to the experimental data compared to the Freundlich model, as evidenced by the R^2 values exceeding 0.99. These compelling findings strongly suggest that the adsorption

Table 2 Adsorption isotherm parameters for MB dye adsorption on BC

Temperature (°C)	Langmuir model				Freundlich model		
	Q_m	K_L	R^2	R_L	n	K_F	R^2
20	169.49	1.294	0.998	$0.009 < R_L < 0.019$	11.84	124.56	0.974
30	234.74	0.901	0.991	$0.013 < R_L < 0.027$	5.14	135.16	0.975
40	250.63	1.789	0.991	$0.007 < R_L < 0.014$	3.98	140.31	0.954

of MB dye by BC predominantly occurs through a monolayer adsorption mechanism on the surface. Moreover, the maximum adsorption capacity, as determined by the Langmuir model, is found to be 250.63 mg g^{-1}, underscoring the remarkable potential of BC for efficiently adsorbing MB dye from the solution.

To further validate the applicability of the Langmuir isotherm in describing the adsorption process, an equilibrium constant R_L was introduced. This parameter provides valuable insight into the type of adsorption occurring. Specifically, when $R_L = 0$, it signifies reversible adsorption; $0 < R_L < 1$ indicates favorable adsorption; $R_L = 1$ represents linear adsorption; $R_L > 1$ suggests unfavorable adsorption.[19] The equation for the equilibrium constant R_L is expressed as eqn (10).

$$R_L = \frac{1}{1 + K_L C_0} \tag{10}$$

where C_0 is the initial concentration and K_L is the Langmuir constant.

In the Langmuir model presented in Table 2, the equilibrium constant R_L values were found to be between 0 and 1. This crucial result indicates that the BC exhibits favorable adsorption characteristics and demonstrates a strong affinity for MB dye.[31] As R_L values within this range signify favorable adsorption, it further supports the notion that the adsorption process can be accurately described by the Langmuir model. These findings strengthen the understanding of the interactions between BC and MB dye, confirming the efficacy of BC as an effective adsorbent for MB dye removal.

3.3.2. Adsorption kinetics of BC for MB dye. This study places significant emphasis on investigating the adsorption mechanism and evaluating the adsorption performance of MB dye on BC. The selection of an appropriate adsorption kinetic model is crucial in achieving these objectives.[32] In this regard, both the pseudo-first-order and pseudo-second-order kinetic models were employed to assess the efficacy of BC in adsorbing MB dye at different time intervals (Fig. 3c). The following expressions of eqn (11) and (12) represent the relevant equations for the non-linear model of adsorption kinetics.[18,33]

$$Q_t = Q_e(1 - e^{-k_1 t}) \tag{11}$$

$$Q_t = \frac{Q_e^2 K_2 t}{1 + K_2 Q_e t} \tag{12}$$

where Q_e and Q_t are the adsorption amounts at equilibrium and at any time t (min) respectively; k_1 is the rate constant for the pseudo-first-order equation (min^{-1}); k_2 is the rate constant for the pseudo-second-order equation (g (mg^{-1} min^{-1})).

The relevant adsorption parameters for the adsorption kinetics can be found in the ESI.† The R^2 values attained for the pseudo-first-order model and pseudo-second-order model were 0.998 and 0.989, respectively. Notably, the pseudo-first-order model accurately predicted a theoretical adsorption capacity of 82.86 mg g^{-1}, which closely aligns with the experimental data of 84.37 mg g^{-1}. These compelling findings suggest that the pseudo-first-order model offers a superior depiction of the sorption behavior of MB dye on BC. The high correlation coefficient (R^2 value) further strengthens the reliability and accuracy of the pseudo-first-order model in describing the adsorption kinetics of MB dye onto BC.

3.3.3. Adsorption thermodynamics of BC for MB dye. The impact of temperature on BC adsorption has been identified as a critical factor by Zhou *et al.*[34] In this study, a comprehensive examination of temperature effects was conducted to analyze the thermodynamic parameters (ΔG, ΔH, and ΔS) governing the capacity, spontaneity, and feasibility of the adsorption process. These thermodynamic parameters were calculated using eqn (5), (6), and (7), respectively.

Fig. 3d illustrates the thermodynamic curves representing the adsorption of MB dye on BC, and the corresponding thermodynamic parameters are provided in the ESI.† The obtained ΔG values at temperatures of 293, 303, 313, 323, and 333 K were all found to be negative, indicating a spontaneous adsorption process. The ΔH values, both positive and negative, indicate heat absorption and an exothermic nature of the adsorption process.[18] As shown in Table S6,† the positive ΔH value implies that BC absorbs heat during the adsorption process.[35] Moreover, as the temperature increases, the kinetic energy and diffusivity of MB dye molecules rise, promoting their movement towards the adsorption sites on BC. The positive ΔS value signifies an increased affinity of BC for MB dye and impacts the stoichiometry of the adsorption process.[24,36]

3.3.4. Effect of pH on the adsorption of MB dye by BC. Fig. 4a illustrates the impact of MB dye solution pH on BC adsorption. The data clearly demonstrated that the adsorption of MB dye on BC intensifies with an increase in solution pH, particularly showing higher adsorption in alkaline environments compared to acidic ones. This behavior can be attributed to the cationic nature of MB dye in the solution. At lower pH levels, the increased presence of H^+ ions competes with MB cations for the active adsorption sites on the BC surface.[37] As the pH value rises, the concentration of OH^- ions increases. When the pH surpasses the zero-point potential of the BC surface, the surface becomes negatively

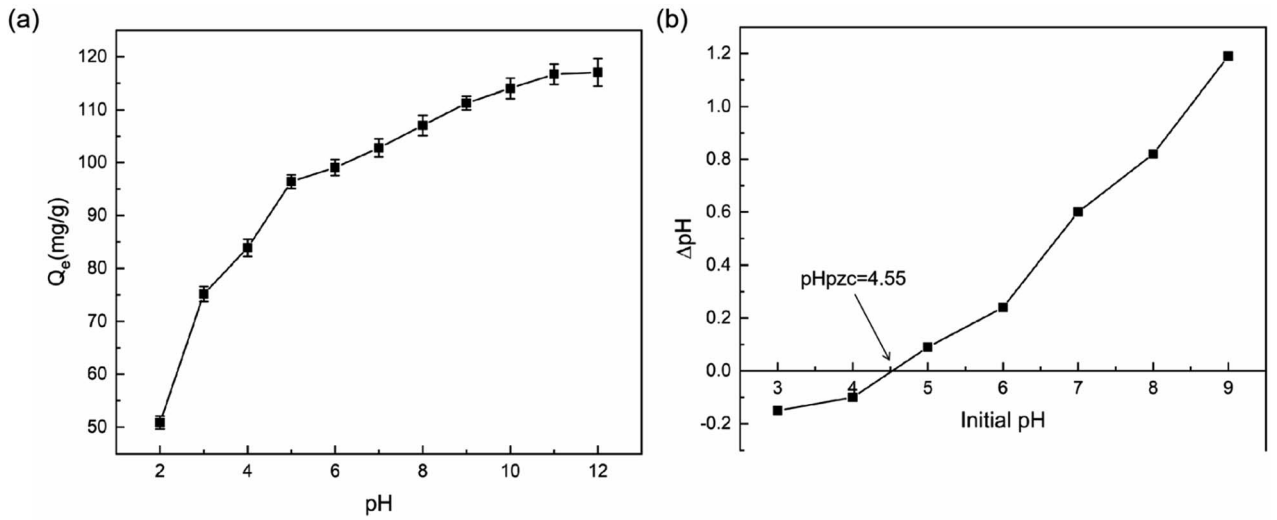

Fig. 4 (a) Effect of pH on the adsorption of MB dye by BC and (b) pH_{pzc} of BC.

charged. This negative charge facilitates an attractive electrostatic interaction with MB cations in the solution, leading to a strengthened adsorption of MB dye on the BC surface.

3.3.5. Adsorption mechanism of MB dye on BC. As depicted in Fig. 7, the adsorption mechanism of MB dye by BC predominantly involves surface adsorption, electrostatic interactions, hydrogen bonding, and π–π interactions. In this study, we conducted an in-depth analysis of the adsorption mechanism by considering critical factors such as the surface charge, chemical structure, pore size, and surface area of BC.

The pH_{pzc} is a crucial parameter that determines the pH value at which a solid surface carries no net charge in an aqueous solution. For BC, the positive or negative charges on its surface depend on the pH value of the MB dye solution.[22] The measured pH_{pzc} of BC is 4.55. When the pH of the MB dye solution is lower than the pH_{pzc} of BC, the surface of BC carries a positive charge, making it more favorable for adsorbing anions. Conversely, when the pH of the MB dye solution is higher than the pH_{pzc}, the net charge on the BC surface becomes negative, enhancing its ability to adsorb cations.[38] The magnitude of the pH_{pzc} reflects the nature of functional groups present on the surface of BC to some extent. It also explains that under alkaline conditions, the acid–base properties of the BC surface will be stronger than those of the MB dye solution surface. This, in turn, accounts for the improved adsorption of BC under alkaline conditions compared to acidic conditions.

The remarkable adsorption capacity of MB dye on BC can be attributed to its substantial surface area and distinctive microporous structure. This is evident from the N_2 adsorption–desorption isotherms and pore size distribution curves shown in Fig. 5a. At a relative pressure (P/P_0) below 0.2, the N_2 adsorption exhibits a rapid increase as the microporous channels within BC begin to fill with N_2. As the relative pressure further increases, N_2 adsorption reaches saturation, leading to multi-molecular layer adsorption and the formation of a hysteresis loop. These observations align with previous literature.[39] Notably, as the relative pressure (P/P_0) approaches 1, the isotherm demonstrates an upward trend, indicating the presence of a macroporous structure within BC.[39] Based on the IUPAC classification, the N_2 adsorption–desorption isotherms of BC in this study fall under type IV,[40] indicating the presence of a well-developed mesoporous structure. From the SEM image of BC in Fig. 6, it can also be found that the surface of BC is rough and inhomogeneous with some cracks and holes of different sizes, which may be because the atomic diameter of Zn atoms is relatively large during the activation process of $ZnCl_2$, and a larger number of micropores are produced during acid washing after activation, and sufficient pore size is favorable for the adsorption of MB dyes. Furthermore, the pore size distribution diagram reveals that the pore structure is primarily composed of micropores, with a certain proportion of mesopores and macropores, contributing to the overall adsorption capacity of MB dye on BC.

To investigate the adsorption of MB dye on the surface functional groups of BC, FTIR spectroscopy was employed, analyzing both the absorbed and unabsorbed BC samples. The FTIR spectrum of BC, as shown in Fig. 5b, exhibits a peak at 3434 cm^{-1} corresponding to the stretching vibration of hydroxyl functional groups (OH^-) present on the BC surface. After the adsorption of MB dye on BC, two new peaks appear in the BC-MB spectrum at 1143 cm^{-1} and 1022 cm^{-1}. These peaks can be attributed to the C–O stretching vibrations of ester and ether bonds, along with the C=O stretching vibrations of carboxylic groups.[37] Additionally, peaks observed at 881 cm^{-1} indicate the presence of C–N bonds and aromatic C–H bonds. Notably, the stretching of C–N bonds and the shifting of aromatic C–H bonds are attributed to the adsorption of MB dye on BC.[20] Furthermore, FTIR spectroscopy reveals the manifestation of the N–H stretching vibration at 1571 cm^{-1}.[37] Overall, the FTIR spectroscopy results provide valuable insights into the adsorption mechanism of MB dyes by BC, indicating the involvement of hydrogen bonding and π–π interactions.[41]

In addition to the FTIR spectroscopy analysis, the structural properties of the BC used in our study were compared with those of coconut activated carbon (CAC) based on literature reports (see

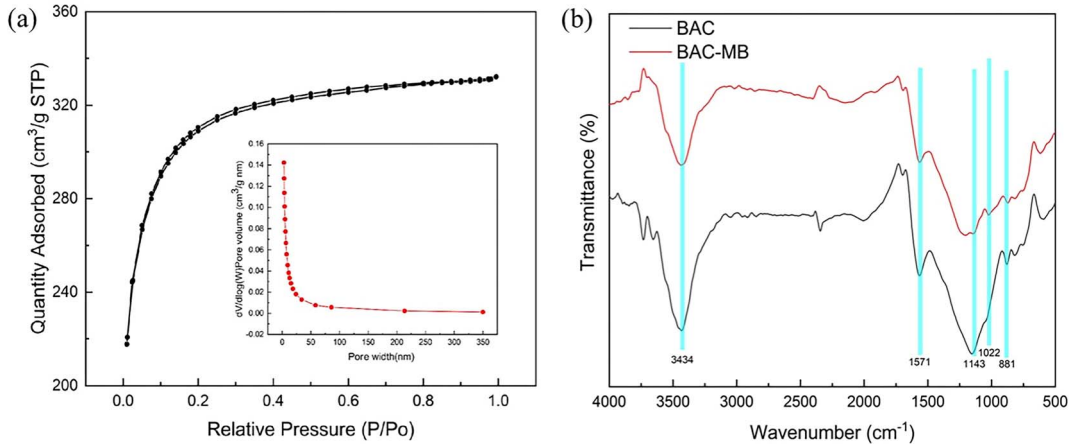

Fig. 5 (a) N_2 adsorption–desorption isotherms and pore size distribution curves of BC and (b) infrared spectra of BC before and after adsorption of MB dye.

the ESI†).[42] The BC exhibited a remarkable surface area of 1134.619 $m^2\ g^{-1}$ and a total pore volume of 0.514 $cm^3\ g^{-1}$. Within this total pore volume, 0.447 $cm^3\ g^{-1}$ was attributed to micropores, while 0.067 $cm^3\ g^{-1}$ was attributed to mesopores. The prevalence of micropores in the BC significantly contributed to its larger specific surface area and enhanced adsorption capacity. Importantly, the BC exhibited significantly higher surface area and pore volume in comparison to CAC. This improvement can be attributed to the activation process involving $ZnCl_2$. During activation, hydrogen and oxygen were eliminated from the biomass, releasing as water vapor, which in turn led to the development of a porous structure.[43] Additionally, $ZnCl_2$ acted as a framework during the activation process, facilitating the formation and accumulation of char. Subsequent acid washing effectively removed the $ZnCl_2$, resulting in an increase in the surface area and voids, leading to the formation of highly porous biochar.[44] The synergistic effects of these processes contributed to the exceptional structural properties of the BC used in our study.

3.4. Mass balance of the entire process

Fig. 8 presents the comprehensive mass balance of the entire production process, detailing the distribution and flow of mass at each stage involved in the production of FF and BC, starting from the initial 100 g of *C. oleifera* husks subjected to dilute HA pretreatment.

Initially, the *C. oleifera* husks contain 22.6 g of cellulose, 36.4 g of hemicellulose, and 38.9 g of lignin per 100 g. After the dilute HA pretreatment, all the hemicellulose is removed and hydrolyzed, resulting in the production of 29.3 g of aqueous xylose solution. Simultaneously, a solid residue is obtained, consisting of 21.1 g of cellulose and 30.1 g of lignin. The solid–liquid separation process yields a filtrate, which is then catalyzed with 15.0 g per L $MgCl_2$ at 180 °C for 1.5 h. This catalytic reaction leads to the production of 21.2 g of FF. Subsequently, the FF undergoes further treatment using S-8 macroporous resin adsorption and 2-Me-THF, resulting in the final yield of 11.3 g of FF. On the other hand, the filtrate obtained from the solid–liquid separation step is subjected to activation at 500 °C with 4 mol per L $ZnCl_2$ and carbonized for 3 h. This process yields 29.7 g of BC.

Importantly, the entire process is conducted without any waste liquid or residue discharge, exemplifying the adherence to the green and environmentally friendly biomass conversion concept. This mass balance demonstrates an efficient utilization of the raw material while minimizing waste and environmental impact.

3.5. Comparison with other relevant research in the literature

Tables 3 and 4 present the removal rates of hemicellulose and the yield of fermentable sugars (FF) achieved through various pretreatment methods, including CO_2 gas explosion, ionic liquids, organic solvents, and others. From Table 3, it is

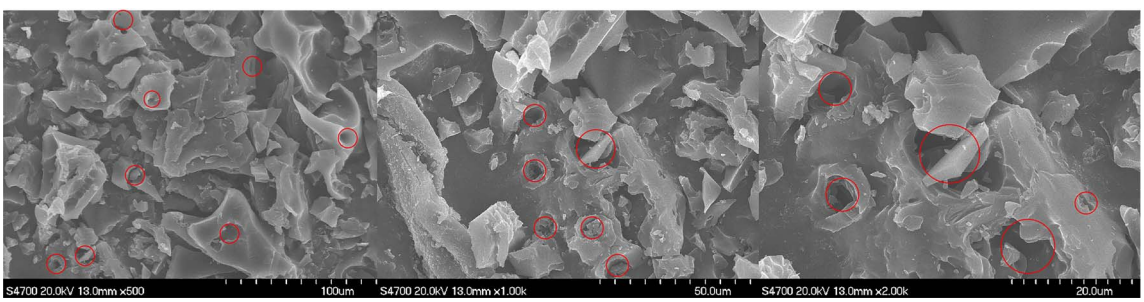

Fig. 6 SEM image of BC.

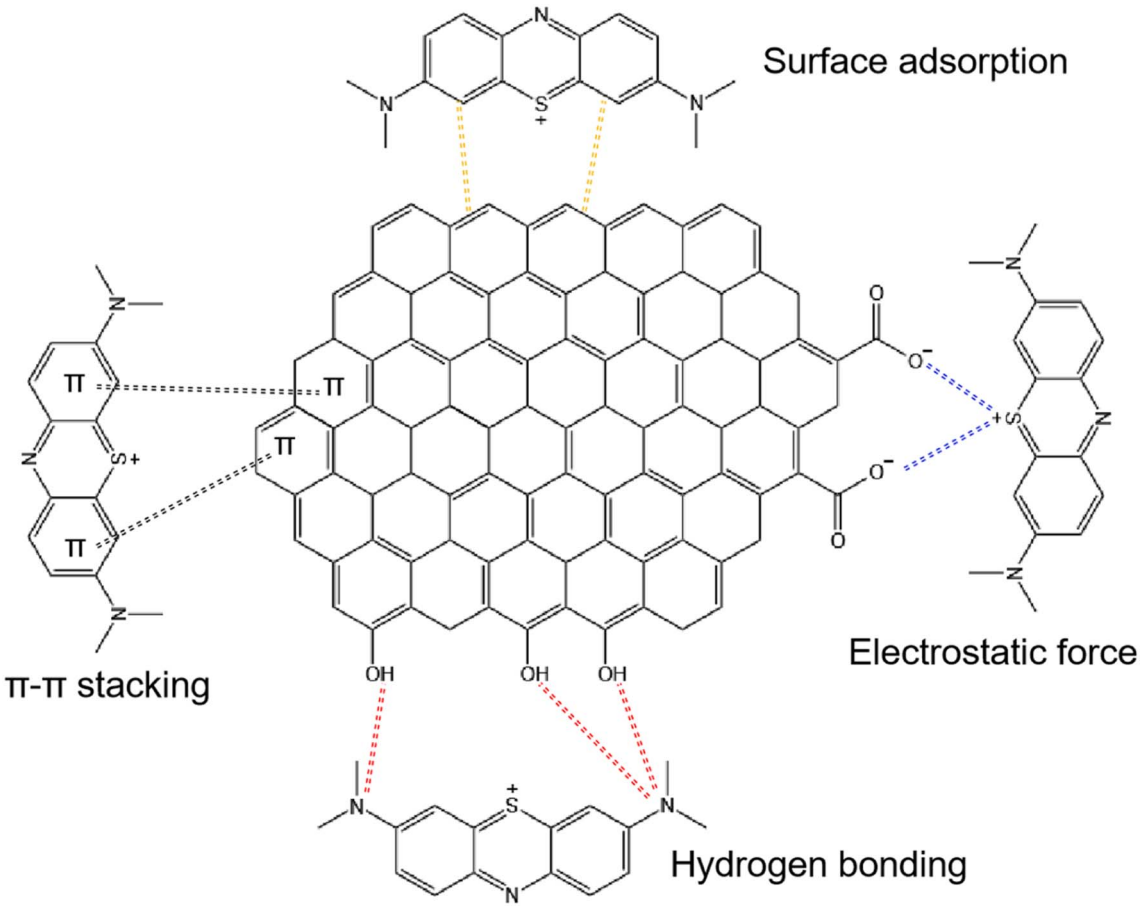

Fig. 7 Schematic mechanism for the high adsorption capacity of MB dye on BC.

evident that hemicellulose can be effectively removed through high-temperature treatment within specific time frames. Hemicellulose, being the least resistant of the lignocellulosic components, exhibits greater susceptibility to removal at relatively high temperatures and under acidic or alkaline conditions. In this study, a 10% dilute HA solution at 130 °C

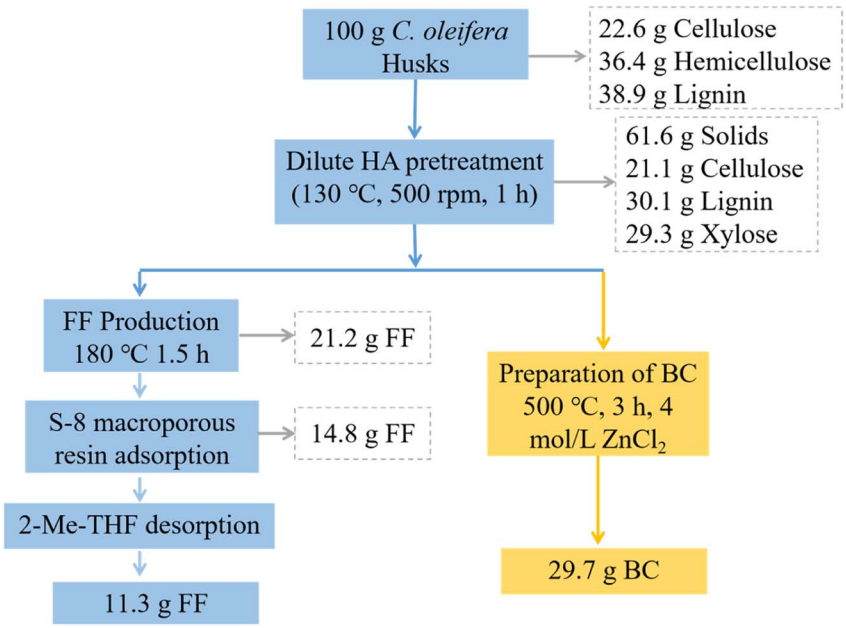

Fig. 8 Mass balance of FF and BC produced from 100 g of *C. oleifera* husks after pretreatment with dilute HA.

Table 3 Comparison of different pretreatment methods for hemicellulose removal

Approaches	Conditions	Hemicellulose removal (%)	References
1-Butyl-3-methylimidazolium hydrogen sulphate ionic liquid	160 °C, 70 min, 10% (wt%)	100	48
High pressure CO_2–H_2O	180 °C, 45 min, 10% (wt%), 35 bar	90.58	49
ChCl : OA : EG DES[a]	100 °C, 180 min	79.7	50
GVL	160 °C, 60 min, 20% (wt%)	98.4	51
Dilute HA	130 °C, 60 min, 20% (wt%)	100	Our work

[a] Choline chloride : oxalic acid : ethylene glycol.

Table 4 Comparison of FF production by different pretreatment methods

Approaches	Conditions	Furfural yield (%)	References
1-Butyl-3-methylimidazolium hydrogen sulfate ([Bmim][HSO_4]) ionic liquid	140 °C, 240 min	82.2	52
1-Ethyl-3-methylimidazolium hydrogen sulfate + vacuum	100 °C, 240 min	82	53
High pressure CO_2–H_2O	180 °C, 60 min, 50 bar	70	54
GVL	180 °C, 10 min	76.6	51
Dilute HA	180 °C, 90 min	72.3	Our work

for 60 min completely removes hemicellulose, while minimally affecting cellulose and lignin contents.

Each pretreatment method has its distinct advantages and disadvantages. For instance, ionic liquids demonstrate excellent performance in dissolving lignocellulosic components, require simple equipment, operate under mild conditions, facilitate recycling, and have negligible pollutant generation. However, synthetic ionic liquids entail considerable costs and challenges in recycling, such as high energy consumption and low recycling rates.[45]

The CO_2 blasting method, operating under high pressure, facilitates cellulase permeation and avoids the production of inhibitory compounds during subsequent hydrolysis and fermentation processes. Nonetheless, this method necessitates expensive equipment, exhibits limited lignin removal effectiveness, and incurs relatively higher economic costs.[46]

In contrast, the acid pretreatment process involves the use of concentrated and dilute acids to disrupt the rigid structure of lignocellulose, enhancing enzymatic hydrolysis and the release of fermentable sugars, ultimately resulting in relatively higher sugar yields.[47] Additionally, the dilute acid solution employed in this study can be recycled, thereby reducing process costs. Nevertheless, the use of dilute acid reagents poses potential hazards due to their toxic and corrosive nature, increasing the risk of vessel corrosion.

Although various lignocellulosic pretreatment technologies exist, each comes with its own set of challenges, such as high costs, low efficiency, harsh operating conditions, and significant environmental pollution, making them unsuitable for immediate industrial implementation. The future trend lies in developing efficient, cost-effective, and environmentally friendly lignocellulose pretreatment technologies to address these shortcomings.

4. Conclusions

In summary, the research investigated the adsorption mechanism of FF using S-8 macroporous resin through comprehensive analyses of adsorption isotherms, kinetics, and thermodynamics. The Langmuir model effectively described the adsorption process with a Q_m value of 335.68 mg g^{-1}, which was found to be spontaneous and exothermic. The resolution of FF was achieved with a 76.1% yield using 2-MeTHF, a low-polarity solvent favoring adsorption. A novel material, BC, showed remarkable adsorption capabilities for MB, following the Langmuir model with a Q_m value of 250.63 mg g^{-1}. BET analysis confirmed BC's large specific surface area, primarily comprising micropores and mesopores. Activation with $ZnCl_2$ further enhanced the surface area and pore size, significantly promoting MB dye adsorption. FTIR analysis revealed the crucial role of hydrogen bonding and π–π interactions in facilitating MB adsorption on BC, which was also confirmed by SEM images. The study also highlighted the recyclability of dilute HA, S-8 macroporous resin, and organic solvent. By emphasizing innovative approaches towards hemicellulose-to-FF conversion and BC production, this research underscored the effective harnessing of the potential of *C. oleifera* husks.

Data availability

Data will be made available on request.

Conflicts of interest

The authors declare no known competing financial interests.

Acknowledgements

This work was financially funded by the National Key Research & Development Plan Project (Grant No. 2022YFB4201801).

References

1 T. Zhang, W. Li, H. Xiao, Y. Jin and S. Wu, Recent progress in direct production of furfural from lignocellulosic residues and hemicellulose, *Bioresour. Technol.*, 2022, **354**, 127126.

2 V. K. Ponnusamya, D. D. Nguyenc, J. Dharmarajad, S. Shobanae, J. R. Banuf, R. G. Saratalegc, S. W. Changc and G. Kumar, A review on lignin structure, pretreatments, fermentation reactions and biorefinery potential, *Bioresour. Technol.*, 2019, **271**, 462–472.

3 M. Y. Hu, L. Yuan, Z. Y. Cai, W. H. Zhang, Q. Fu and D. D. Ji, Ammonia fiber expansion-assisted deep eutectic solvent treatment for wheat straw fraction separation and bioconversion, *Bioresour. Technol.*, 2023, **367**, 128242.

4 S. C. Sun, P. F. Wang, X. F. Cao, S. N. Sun and J. L. Wen, An integrated pretreatment for accelerating the enzymatic hydrolysis of poplar and improving the isolation of co-produced hemicelluloses, *Ind. Crops Prod.*, 2021, 114101.

5 X. J. Shen, J. L. Wen, Q. Q. Mei, C. Xue, D. Sun, T. Q. Yuan and R. C. Sun, Facile fractionation of lignocelluloses by biomass-derived deep eutectic solvent (DES) pretreatment for cellulose enzymatic hydrolysis and lignin valorization, *Green Chem.*, 2019, **21**, 275–283.

6 M. H. L. Silveira, A. R. C. Morais, A. M. da Costa Lopes, D. N. Olekszyszen, R. Bogel-Łukasik, J. Andreaus and L. Pereira Ramos, Current Pretreatment Technologies for the Development of Cellulosic Ethanol and Biorefineries, *ChemSusChem*, 2015, **8**, 3366–3390.

7 H. Zhou, R. Zhang, W. Zhan, L. Wang, L. Guo and Y. Liu, High biomass loadings of 40 wt% for efficient fractionation in biorefineries with an aqueous solvent system without adding adscititious catalyst, *Green Chem.*, 2016, 18.

8 Y. Yu, H. Xu, H. Yu, L. Hu and Y. Liu, Formic acid fractionation towards highly efficient cellulose-derived PdAg bimetallic catalyst for H_(2) evolution, *Green Energy Environ.*, 2022, **7**, 172–183.

9 H. Mashhadimoslem, A. Ghaemi, A. Maleki and A. Elkamel, Enhancement of oxygen adsorption using biomass-based oxidized porous carbon, *J. Environ. Chem. Eng.*, 2023, **11**, 109300.

10 P. Manzanares, The role of biorefinering research in the development of a modern bioeconomy, *Acta Innovations*, 2020, **37**, 47–56.

11 E. Cousin, K. Namhaed, Y. Pérès, P. Cognet, M. Delmas, H. Hermansyah, M. Gozan, P. A. Alaba and M. K. Aroua, Towards efficient and greener processes for furfural production from biomass: A review of the recent trends, *Sci. Total Environ.*, 2022, **847**, 157599.

12 Y. Zhao, K. Lu, H. Xu, L. Zhu and S. Wang, A critical review of recent advances in the production of furfural and 5-hydroxymethylfurfural from lignocellulosic biomass through homogeneous catalytic hydrothermal conversion, *Renewable Sustainable Energy Rev.*, 2021, **139**, 110706.

13 T. T. Ninh, D. K. Dan, N. T. Phuong, N. M. Dat, P. T. Khang, P. P. Bao, L. M. Bao, D. D. Nhan, N. N. Khoa, N. T. Hanh, D. N. Hoa, V. N. D. Viet, T. T. Danh, P. T. L. Chau, M. T. Phong and N. H. Hieu, Sustainable synthesis of cellulose-derived magnetic iron oxide/sulfonated graphene oxide-like material from corncob for conversion of hemicellulose to furfural, *Fuel*, 2023, **343**, 127870.

14 M. N. Catrinck, P. S. Barbosa, H. R. O. Filho, R. S. Monteiro, M. H. P. Barbosa, R. M. Ribas and R. F. Teofilo, One-step process to produce furfural from sugarcane bagasse over niobium-based solid acid catalysts in a water medium, *Fuel Process. Technol.*, 2020, **207**, 106482.

15 K. J. Yong, T. Y. Wu, C. B. T. L. Lee, Z. J. Lee, Q. Liu, J. M. Jahim, Q. Zhou and L. Zhang, Furfural production from biomass residues: Current technologies, challenges and future prospects, *Biomass Bioenergy*, 2022, **161**, 106458.

16 S. Li, Y. Yang, H. Shan, J. Zhao, Z. Wang, D. Cai, P. Qin, J. Baeyens and T. Tan, Ultrafast and ultrahigh adsorption of furfural from aqueous solution via covalent organic framework-300, *Sep. Purif. Technol.*, 2019, **220**, 283–292.

17 H. Xiang, K. Dai, J. Kou, G. Wang, Z. Zhang, D. Li, C. Chen and J. Wu, Selective adsorption of ferulic acid and furfural from acid lignocellulosic hydrolysate by novel magnetic lignin-based adsorbent, *Sep. Purif. Technol.*, 2023, **307**, 122840.

18 H. Xue, X. Wang and Q. Xu, Adsorption of methylene blue from aqueous solution on activated carbons and composite prepared from an agricultural waste biomass:A comparative study by experimental and advanced modeling analysis, *Chem. Eng. J.*, 2022, **430**, 132801.

19 Y. Yang and F. S. Cannon, Biomass activated carbon derived from pine sawdust with steam bursting pretreatment; perfluorooctanoic acid and methylene blue adsorption, *Bioresour. Technol.*, 2022, **344**, 126161.

20 W. Wei, N. Shang, X. Zhang, W. Liu, T. Zhang and M. Wu, A green 3-step combined modification for the preparation of biomass sorbent from waste chestnut thorns shell to efficient removal of methylene blue, *Bioresour. Technol.*, 2022, **360**, 127593.

21 V. Gomase, R. Jugade, P. Doondani, S. Deshmukh, D. Saravanan and S. Pandey, Dual modifications of chitosan with PLK for amputation of cyanide ions: Equilibrium studies and optimization using RSM, *Int. J. Biol. Macromol.*, 2022, **223**, 636–651.

22 S. Pandey, J. Y. Do, J. Kim and M. Kang, Fast and highly efficient removal of dye from aqueous solution using natural locust bean gum based hydrogels as adsorbent, *Int. J. Biol. Macromol.*, 2020, **143**, 60–75.

23 S. Pandey, E. Makhado, S. B. Kim and M. Kang, Recent developments of polysaccharide based superabsorbent nanocomposite for organic dye contamination removal from wastewater, *Environ. Res.*, 2023, **217**, 114909.

24 A. H. Jawad, S. E. M. Saber, A. S. Abdulhameed, A. Reghioua, Z. A. Alothman and L. D. Wilson, Mesoporous activated carbon from mangosteen (Garcinia mangostana) peels by

H3PO4 assisted microwave: Optimization, characterization, and adsorption mechanism for methylene blue dye removal, *Diamond Relat. Mater.*, 2022, **129**, 109389.

25 O. Baytar, O. Sahin and C. Saka, Sequential application of microwave and conventional heating methods for preparation of activated carbon from biomass and its methylene blue adsorption, *Appl. Therm. Eng.*, 2018, **138**, 542–551.

26 Y. Liu, X. Wang, M. Hu and Y. Yu, Catalytic conversion of 2,5-furandicarboxylic acid production from hemicellulose, *Biomass Convers. Biorefin.*, 2023, DOI: **10.1007/s13399-023-04162-4**.

27 A. Sluiter, B. Hames, R. Ruiz, C. Scarlata, J. Sluiter, D. Templaton and D. Crocker, *Determination of Structural Carbohydrates and Lignin in Biomass, Technical Report NREL/TP-510-42618*, National Renewable Energy Laboratory, Golden, CO, 2010.

28 H. Guo, R. Su, R. Huang, W. Qi and Z. He, Co-optimization of sugar yield and input energy by the stepwise reduction of agitation rate during lignocellulose hydrolysis, *Food Bioprod. Process.*, 2015, **95**, 1–6.

29 H. Zhou, R. Zhang, W. Zhan, L. Wang, L. Guo and Y. Liu, High biomass loadings of 40 wt% for efficient fractionation in biorefineries with an aqueous solvent system without adding adscititious catalyst, *Green Chem.*, 2016, **18**, 6108–6114.

30 Q. Lin, Q. Zhan, R. Li, S. Liao, J. Ren, F. Peng and L. Li, Solvent Effect on Xylose-to-Furfural Reaction in Biphasic Systems: Combined Experiments with Theoretical Calculations, *Green Chem.*, 2021, **23**, 8510.

31 Z. Wu, X. Wang, J. Yao, S. Zhan, H. Li, J. Zhang and Z. Qiu, Synthesis of polyethyleneimine modified CoFe2O4-loaded porous biochar for selective adsorption properties towards dyes and exploration of interaction mechanisms, *Sep. Purif. Technol.*, 2021, **277**, 119474.

32 H. Li, J. Kong, H. Zhang, J. Gao, Y. Fang, J. Shi, T. Ge, T. Fang, Y. Shi, R. Zhang, N. Zhang, X. Dong, Y. Zhang and H. Li, Mechanisms and adsorption capacities of ball milled biomass fly ash/biochar composites for the adsorption of methylene blue dye from aqueous solution, *J. Water Process. Eng.*, 2023, **53**, 103713.

33 D. Jiang, H. Li, X. Cheng, Q. Ling, H. Chen, B. Barati, Q. Yao, A. Abomohra, X. Hu, P. Bartocci and S. Wang, A mechanism study of methylene blue adsorption on seaweed biomass derived carbon: From macroscopic to microscopic scale, *Process Saf. Environ. Prot.*, 2023, **172**, 1132–1143.

34 Y. Zhou, Z. Liang, J. Wen, T. Liu, J. J. Dong, C. Chang, X. Zheng and W. Zheng, Ternary Mg-B-S co-modified Ficus virens biochar for ultra-high adsorption of rhodamine B in lab-scale and field-scale application: Adsorption behavior and mechanisms, *Ind. Crops Prod.*, 2023, **194**, 116310.

35 S. K. Theydan and M. J. Ahmed, Adsorption of methylene blue onto biomass-based activated carbon by FeCl3 activation: Equilibrium, kinetics, and thermodynamic studies, *J. Anal. Appl. Pyrolysis*, 2012, **97**, 116–122.

36 Z. Wu, X. Wang, J. Yao, S. Zhan, H. Li, J. Zhang and Z. Qiu, Synthesis of polyethyleneimine modified CoFe2O4-loaded porous biochar for selective adsorption properties towards dyes and exploration of interaction mechanisms, *Sep. Purif. Technol.*, 2021, **277**, 119474.

37 X. Fan, L. Peng, X. Wang, S. Han, L. Yang, H. Wang and C. Hao, Efficient capture of lead ion and methylene blue by functionalized biomass carbon-based adsorbent for wastewater treatment, *Ind. Crops Prod.*, 2022, **183**, 114966.

38 K. Ravichandran, N. Siva Jyothi, K. Thirumurugan, S. Suvathi, N. Chidhambaram, R. Uma and B. Sundaresan, Influence of Mo + F incorporation and point of zero charge on the dye degradation efficacy of ZnO thin films, *Chem. Phys.*, 2023, **564**, 111714.

39 D. Pandey, A. Daverey, K. Dutta, V. K. Yata and K. Arunachalam, Valorization of waste pine needle biomass into biosorbents for the removal of methylene blue dye from water: Kinetics, equilibrium and thermodynamics study, *Environ. Technol. Innovation*, 2022, **25**, 102220.

40 G. Li, J. Li, W. Tan, M. Yang, H. Wang and X. Wang, Effectiveness and mechanisms of the adsorption of carbendazim from wastewater onto commercial activated carbon, *Chemosphere*, 2022, **304**, 135231.

41 L. Wu, X. Zhang and Y. Si, Polydopamine functionalized superhydrophilic coconut shells biomass carbon for selective cationic dye methylene blue adsorption, *Mater. Chem. Phys.*, 2022, **279**, 125767.

42 S. Sybounya and R. Nitisoravut, Hybrid composite of modified commercial activated carbon and Zn-Ni hydrotalcite for fermentative hydrogen production - ScienceDirect, *J. Environ. Chem. Eng.*, 2020, **9**, 104801.

43 H. K. Yagmur and I. Kaya, Synthesis and characterization of magnetic ZnCl2-activated carbon produced from coconut shell for the adsorption of methylene blue, *J. Mol. Struct.*, 2021, 1232.

44 Y. X. Seow, Y. H. Tan, N. M. Mubarak, J. Kansedo, M. Khalid, M. L. Ibrahim and M. Ghasemi, A review on biochar production from different biomass wastes by recent carbonization technologies and its sustainable applications, *J. Environ. Chem. Eng.*, 2022, **10**, 107017.

45 J. Afonso, A. Mezzetta, I. M. Marrucho and L. Guazzelli, History repeats itself again: Will the mistakes of the past for ILs be repeated for DESs? From being considered ionic liquids to becoming their alternative: the unbalanced turn of deep eutectic solvents, *Green Chem.*, 2023, **25**, 59–105.

46 J. Dharmaraja, S. Shobana, S. Arvindnarayan, R. R. Francis, R. B. Jeyakumar, R. Saratale, A. K. Veeramuthu, S. K. Bhatia, V. Kumar and G. K. J. K. P. Envelope, Lignocellulosic biomass conversion via greener pretreatment methods towards biorefinery applications, *Bioresour. Technol.*, 2023, **369**, 128328.

47 J. Singh, M. Suhag and A. Dhaka, Augmented digestion of lignocellulose by steam explosion, acid and alkaline pretreatment methods: A review, *Carbohydr. Polym.*, 2015, **117**, 624–631.

48 A. V. Carvalho, A. e. M. d. C. Lopes and R. Bogel-Łukasik, Relevance of the acidic 1-butyl-3-methylimidazolium hydrogen sulphate ionic liquid in the selective catalysis of

the biomass hemicellulose fraction, *RSC Adv.*, 2015, **5**, 47153.

49 F. M. Relvas, A. R. C. Morais and R. Bogel-Lukasik, Selective hydrolysis of wheat straw hemicellulose using high-pressure CO2 as catalyst, *RSC Adv.*, 2015, **5**, 73935–73944.

50 C. J. Duan, X. Han, Y. H. Chang, J. Xu, G. L. Yue, Y. Zhang and Y. J. Fu, A novel ternary deep eutectic solvent pretreatment for the efficient separation and conversion of high-quality gutta-percha, value-added lignin and monosaccharide from Eucommia ulmoides seed shells, *Bioresour. Technol.*, 2022, **370**, 128570.

51 D. Ding, J. Hu, L. Hui, Z. Liu and L. Shao, Valorization of Miscanthus × giganteus by γ-Valerolactone/H2O/FeCl3 system toward efficient conversion of cellulose and hemicelluloses, *Carbohydr. Polym.*, 2021, **270**, 118388.

52 S. Peleteiro, C. L. Da, M. Andre, G. Garrote, J. C. Parajó and R. Bogel-Ukasik, Simple and Efficient Furfural Production from Xylose in Media Containing 1-Butyl-3-Methylimidazolium Hydrogen Sulfate, *Ind. Eng. Chem. Res.*, 2015, **54**, 8368–8373.

53 S. Lima, P. Neves, M. M. Antunes, M. Pillinger, N. Ignatyev and A. A. Valente, Conversion of mono/di/polysaccharides into furan compounds using 1-alkyl-3-methylimidazolium ionic liquids, *Appl. Catal., A*, 2009, **363**, 93–99.

54 R. Bogel-Lukasik, A. Morais and C. Rita, Highly efficient and selective CO2-adjunctive dehydration of xylose to furfural in aqueous media with THF, *Green Chem.*, 2016, **18**, 2331.